International Journal of Nanomedicine

Dovepress
open access to scientific and medical research

Open Access Full Text Article

ORIGINAL RESEARCH

Biomimetic Iron-Based Nanoparticles Remodel Immunosuppressive Tumor Microenvironment for Metabolic Immunotherapy

Wenyu Zhang[1,*], Linquan Li[1,*], Yaguang Wu[1], Chengzhilin Li[1], Zi'ang Xu[1], Nianlei Zhang[1], Xinyu Wang[1], Yingchun Zhao[1], Tingjian Zu[1], Qingbin He[1], Jianwei Jiao[2], Runxiao Zheng[1]

[1]School of Clinical and Basic Medical Sciences, Medical Science and Technology Innovation Center, Shandong Provincial Hospital, Shandong First Medical University & Shandong Academy of Medical Sciences, Jinan, 250000, People's Republic of China; [2]State Key Laboratory of Stem Cell and Reproductive Biology, Institute of Zoology, Chinese Academy of Sciences, Beijing, 100101, People's Republic of China

*These authors contributed equally to this work

Correspondence: Runxiao Zheng, Medical Science and Technology Innovation Center, Shandong First Medical University & Shandong Academy of Medical Sciences, Jinan, 250000, People's Republic of China, Email zhengrunxiao@sdfmu.edu.cn; Jianwei Jiao, State Key Laboratory of Stem Cell and Reproductive Biology, Institute of Zoology, Chinese Academy of Sciences, Beijing, 100101, People's Republic of China, Email jwjiao@ioz.ac.cn

Introduction: Immunotherapy has led to a paradigm shift in reinvigorating treatment of cancer. Nevertheless, tumor associated macrophages (TAMs) experience functional polarization on account of the generation of suppressive metabolites, contributing to impaired antitumor immune responses.

Methods: Hence, metabolic reprogramming of tumor microenvironment (TME) can synergistically improve the efficacy of anti-tumor immunotherapy. Herein, we engineered an iron-based nanoplatform termed $_{ER}Fe_3O_4$ NPs. This platform features hollow Fe_3O_4 nanoparticles loaded with the natural product emodin, the outer layer is coated with red blood cell membrane (mRBCs) inserted with DSPE-PEG2000-galactose. This effectively modulates lactate production, thereby reversing the tumor immune suppressive microenvironment (TIME).

Results: The $_{ER}Fe_3O_4$ NPs actively targeted TAMs on account of their ability to bind to M2-like TAMs with high expression of galectin (Mgl). $_{ER}Fe_3O_4$ NPs achieved efficient ability to reverse TIME via the production of reducing lactate and prompting enrichment iron of high concentrations. Furthermore, $_{ER}Fe_3O_4$ NPs resulted in heightened expression of CD16/32 and enhanced TNF-α release, indicating promotion of M1 TAMs polarization. In vitro *and* in vivo experiments revealed that $_{ER}Fe_3O_4$ NPs induced significant apoptosis of tumor cells and antitumor immune response.

Discussion: This study combines Traditional Chinese Medicine (TCM) with nanomaterials to synergistically reprogram TAMs and reverse TIME, opening up new ideas for improving anti-tumor immunotherapy.

Keywords: metabolic immunotherapy, nanoparticles, reprograming, iron oxide, macrophages

Introduction

Cancer immunotherapy that activates the host immune system to fight against cancer in a safe and effective manner has attracted tremendous attention.[1–3] However, the highly complex tumor immunosuppressive microenvironment (TIME) governed by malignant cells, stromal cells, and infiltrating immune cells restricts the response of solid tumors to immunotherapy, limiting the number (≈20%) of patients responding to immunotherapy.[4–6] Of these, tumor associated macrophages (TAMs), accounted for up to 50% of some solid neoplasms, are usually the most abundant and typical resident immunosuppressive cells in tumor microenvironment (TME).[7,8] In progressive tumors, the prevalent M2-like TAMs in TME play a crucial role in supporting tumor progression and metastasis. They contribute to various processes such as providing nutritional support, promoting immune escape, facilitating angiogenesis, and influencing tissue remodeling.[9] The immunosuppressive effect of TAMs is primarily mediated through their ability to directly suppress T cells and NK cells.[10] This

Received: 11 June 2024
Accepted: 27 August 2024
Published: 10 September 2024

Graphical Abstract

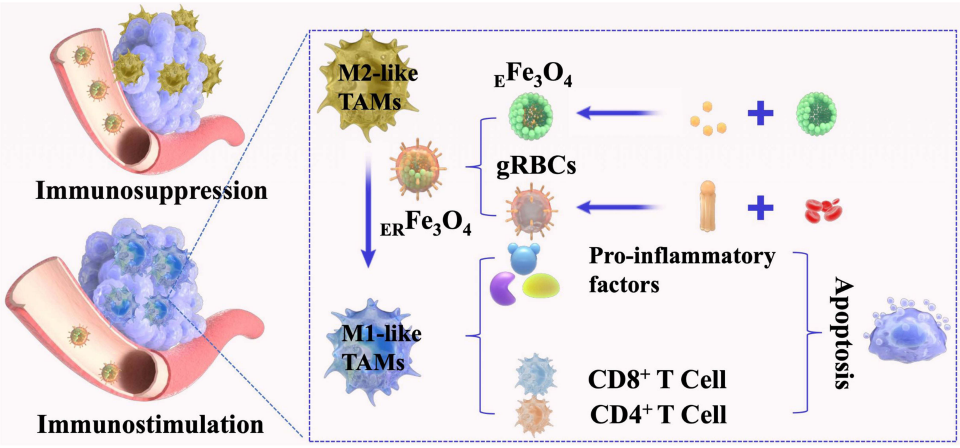

suppression is largely facilitated by the secretion of cytokines such as interleukin-10 (IL-10) and transforming growth factor-β (TGF-β), which are known to dampen T cells immune responses. TAMs also contribute to the enhancement of Tregs' immunosuppressive functions and inhibit dendritic cells (DCs) maturation through interactions mediated by these cytokines.[11] Conversely, transitioning from an M2-like TAMs to an M1-like TAMs phenotype reduces Arg-1, IL-10 and TGF-β secretion while increasing production of tumor necrosis factor-α (TNF-α), interleukin 12 (IL-12) and Interferon-γ (IFN-γ). This phenotypic shift promotes activation of T cells immune responses facilitates DCs maturation, and consequently impedes tumor progression.[12] Moreover, these TAMs can also impact the effectiveness of cancer therapies.[13] Reprogramming M2-like TAMs to M1-like TAMs can improve Th1 expression of IL-12, IFN-γ, and TNF-α and the associated Th1 immune response to restrain tumor growth.[14] Consequently, how to reset TAMs for ameliorating tumor immunosuppression and enhancing T-cell antitumor immunity is a crucial step for the improvement of cancer immunotherapy.

Cancer cells can hijack the function of tumor-infiltrating immune cells to gain benefits for their invasion and metastasis by utilizing metabolic byproducts.[15] The accumulation of lactic acid secreted by cancer cells glycolysis can be precisely sensed by TAMs, leading to the functional polarization of macrophages and the progression of tumors.[16] Based on this, inhibiting lactate accumulation in TME is a promising approach to reshape TAMs and restore tumor immunity. Emodin (1,3,8-trihydroxy-6-methylanthraquinone) is a natural anthraquinone found in various Chinese herbs, such as Rheum palmatum, Polygonum cuspidatum, and Polygonum multiflorum. Several preclinical studies have shown that emodin possesses a broad range of pharmacological benefits, including anti-inflammatory and anti-tumorigenic properties.[17,18] At the end of the glycolysis process, ingested glucose is preferentially decomposed into pyruvic acid through a series of transformations, and finally into lactic acid catalyzed by lactate dehydrogenase (LDH).[19] Targeting LDH inhibition presents a novel strategy in cancer treatment due to its association with the unique glycolytic metabolism found in many aggressive tumor cells.[20] Emodin has been reported to exhibit significant LDH inhibitor activity.[21] There have also been studies reporting that emodin can induce the transformation of M2-like TAMs into M1-like TAMs, thereby inhibiting the proliferation and invasion of tumor cells mediated by co culture with M2-like TAMs.[22] However, the limited solubility of emodin significantly hampers its bioavailability, resulting in low tumor accumulation and uptake of TAMs in vivo. Hence, an effective delivery system to target TAMs in solid tumor and synergistically promote macrophage polarization for tumor immunotherapy is crucial adjective.

In addition, iron and reactive oxygen species (ROS) of high concentrations in TAMs may also play a critical role in macrophage polarization.[23] Previous studies have reported that ferumoxytol, an iron supplement approved by the US Food and Drug Administration (FDA), can trigger a pro-inflammatory immune response through the polarization of M1 macrophages.[24] It has been reported that hollow iron oxide (Fe_3O_4) nanoparticles (NPs) can facilitate the conversion of M2 phenotype to M1 phenotype, leading to increased expression of Th1 cytokines, such as IL-12, IFN-γ, TNF-α and reactivate Th1 immune-

response.[14] It has also been reported that profoundly activated M1-like TAMs are capable of reprogramming neighboring M2-like TAMs into M1-like TAMs via cytokine-mediated intercellular communication.[25] Nevertheless, it is well known that nanoparticles are easily cleared by the reticuloendothelial system during long-term circulation.[26] Erythrocyte membrane coated nanoparticles can "compensate" for the biological interface between the nanoparticles and red blood cells, thereby reducing the clearance of the nanoparticles by the immune system.[23,27] In addition, on account of high level expression of galactose lectin (Mgl) in M2-like TAMs,[28,29] DSPE-PEG-Gala (galactose) inserted erythrocyte membrane can efficiently transport nanoparticles into TAMs, thus enabling the polarization of M2-like TAMs.[30,31]

Herein, we engineered a DSPE-PEG2000-Gala-inserted erythrocyte membrane (gRBCs) cloaked hollow Fe_3O_4 NPs based nanoplatform encapsulating emodin to reverse TIME for antitumor immunotherapy. As illustrated in Figure 1, emodin was introduced to hollow Fe_3O_4 NPs and gRBCs coating on the nanocomplex ($_EFe_3O_4$ NPs) to obtain $_{ER}Fe_3O_4$ NPs for TME remodeling. gRBCs can well recognize Mgl on the surface of M2-like TAMs, thereby efficiently

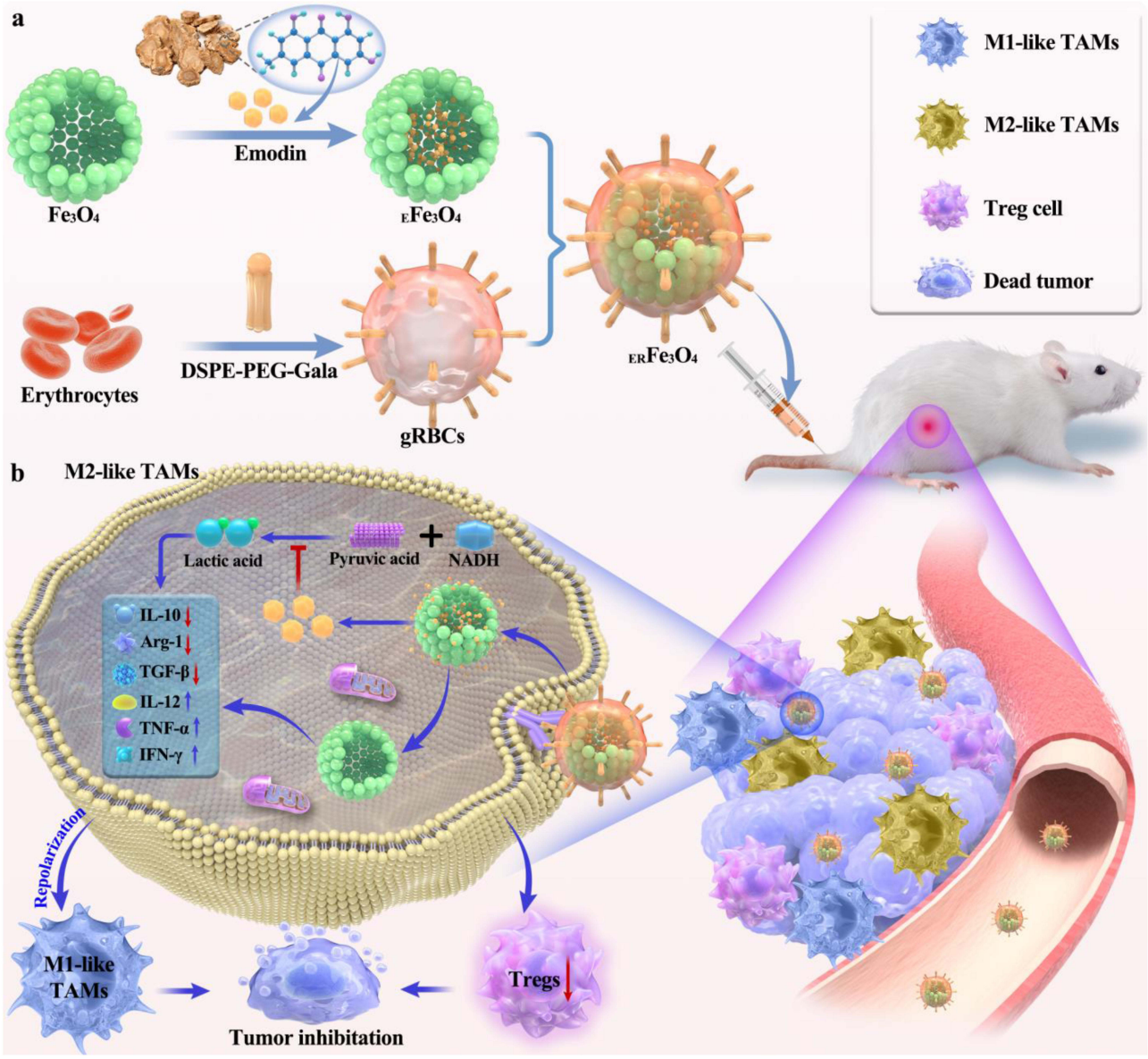

Figure 1 Schematic diagram of $_{ER}Fe_3O_4$ NPs for tumor immunotherapy. (**a**) $_EFe_3O_4$ NPs was prepared by loading emodin with hollow Fe_3O_4 NPs, which was further encapsulated by gRBCs to obtain $_{ER}Fe_3O_4$ NPs. (**b**) The $_{ER}Fe_3O_4$ NPs could target TAMs by binding to M2-like TAMs with high expression of galectin (Mgl). The release of emodin inhibited the production of lactate, with which Fe_3O_4 NPs synergistically to reprogram M2 TAMs into M1 TAMs for eliminating tumors.

transporting $_{E}Fe_3O_4$ NPs into TAMs. The release of emodin can significantly inhibit pyruvic acid transformations into lactate, further restraining and neutralizing tumor acidification to reshape TAMs. Additionally, hollow Fe_3O_4 NPs ulteriorly switch M2-like TAMs into M1-like TAMs, which up-regulate IL-12 and TNF-α secreted by M1-like TAMs and activate and recruit $CD8^+$ and $CD4^+$ T cells to attack tumor cells. Taken together, the $_{ER}Fe_3O_4$ NPs not only facilitate the efficient delivery of emodin to inhibit lactate accumulation but also synergistically induce the transition of M2 TAMs to M1 TAMs, thus enhancing cancer immunotherapy.

Materials and Methods

Materials

Sodium citrate, ferric (III) chloride hexahydrate, polyacrylamide and carbamide, were procured from Sinopharm Chemical Reagent Co., Ltd. Emodin was purchased from Shanghai Yuanye Biologics. DSPE-PEG2000-galactose was purchased from Xi'an Qiyue Biologics. The following reagents were obtained from Biolegend (San Diego, CA, USA): FITC anti-mouse F4/80 antibody, PE anti-mouse CD4 antibody, APC anti-mouse CD8 antibody, PE/Cy7 anti-mouse CD 16/32 antibody, PE anti-mouse CD 206 antibody, mouse IL-10 and mouse TNF-α ELISA kit. The annexin V-FITC apoptosis assay kit and Pyruvic acid kit were provided by Solaibao (China), the Calcein/PI Cell Viability/Cytotoxicity Assay kit and Easy II Protein Quantitative Kit (BCA) was sourced from Beyotime (China), and the petri dishes used for cell culture were obtained from SAINING Biotech (China). 0.4 μm cell embedding dish was purchased from Guangzhou Jet Biotech. Analytical grade chemicals were utilized without the need for additional purification.

Synthesis of Hollow Fe_3O_4 NPs

Briefly, a solution containing 0.54 g of iron (III) chloride hexahydrate, 0.865 g of sodium citrate, and 0.36 g of carbamide dispersed in 40 mL of distilled water was prepared. Slow addition of 0.3 g polyacrylamide allowed for complete dissolution through stirring. The solution was then reacted at 200°C for 12 h.[32] Upon reaching room temperature, the solution was subjected to centrifugation to isolate the black precipitate. The resulting precipitate was washed thrice to remove any unreacted materials and then dried under vacuum conditions at 60°C overnight to obtain the final product.

Preparation of $_{E}Fe_3O_4$ NPs

A solution of 8.5 mg emodin in 2 mL ethanol was prepared and subjected to 10 min of ultrasonication. Simultaneously, a solution of 8 mg hollow Fe_3O_4 NPs in 1 mL ethanol was prepared and thoroughly ultrasonicated for 30 min. The above two solutions were mixed and kept stirring at room temperature for 24 h. The supernatant was centrifuged to calculate the loading efficiency of emodin. The $_{E}Fe_3O_4$ NPs was centrifuged and dried under vacuum at 60°C.[33,34]

Synthesis of $_{ER}Fe_3O_4$ NPs

Whole blood was collected from healthy mice and centrifuged at 3000 rpm for 10 min at 4°C to remove plasma and buffer from whole blood. It was then washed three times with cold phosphate buffered saline (PBS, pH 7.4). The resulting red blood cells (RBCs) are resuspended in 2 mL of ultrapure water for at least 2 h to induce RBC rupture. Afterward, the released hemoglobin was removed by centrifugation at 9000 rpm for 10 min and the supernatant was washed with 1×PBS until colorless. The resulting red blood cell membrane (mRBCs) was finally suspended in 1 mL of 1×PBS.[35] Finally, the obtained mRBCs was quantified using the Easy II Protein Quantitative Kit (BCA) and kept at -80°C until use.[36] Then, 100 μg of DSPE-PEG-Gala was incubated with mRBCs for 30 min to form gRBCs, 200 nm gRBCs were prepared by extruding through a 200 nm filter membrane using a 1 mL syringe.[27] Finally, 1 mL of $_{E}Fe_3O_4$ NPs (0.5 mg mL^{-1}) was mixed with 0.5 mg of gRBCs (total protein) under sonication for 1 min to form $_{ER}Fe_3O_4$ NPs through a 200 nm filter membrane.

Characterization of $_{ER}Fe_3O_4$

Transmission electron microscopy (TEM) images were performed at a 120 kV acceleration voltage by HT7800. Images of the scanning electron microscope (SEM) were obtained using a ZEISS Sigma300 SEM. Crystal structure

measurements were performed with an Ultima IV X-ray diffractometer (XRD, Bruker D8 ADVANCE/Ultima IV, Germany) at 8° min^{-1} using Cu Kα radiation (λ=0.15405 nm, 40KV, 40 mA). X-ray photoelectron spectroscopy (XPS) was also conducted on hollow Fe_3O_4 NPs using a Thermo Scientific K-alpha X-ray Photoelectron Spectrometer System (hv=1486.6 eV). STEM and the elemental mapping images of hollow Fe_3O_4 NPs were obtained by (TALOS F200, FEI, America). The size and Zeta potential of the nanoparticles were determined using a Nano-ZS zetasizer (Nanolink SZ901).[37]

Evaluation of the Inhibitory Effect of Lactate Dehydrogenase

The assays were performed utilizing 40 μM NADH and 200 μM pyruvate, in combination with either 0.66 ng or 0.38 mU of the enzyme, within a final volume of 200 μL (one unit of the enzyme reduces 1 μM of pyruvate to L-lactate at 37°C and pH 8.55). To generate a concentration-response curve, we employed five different concentrations of the compound. The compound solutions (8 μL) were dispensed in 96-well plates. Subsequently, the substrate and cofactor, dissolved in the buffer (152 μL), and the enzyme solution (40 μL) were added.[20] The absorbance of NADH was detected.[38] The measurements adhered to the guidelines provided by the manufacturer of the pyruvate kit.

Cell Culture

Mouse breast cancer cells 4T1 cells and Raw 246.7 cells were all derived from Wuhan Pricella Biotechnology Co. RAW264.7 and 4T1 cells were incubated in 1640 medium containing bispecific antibodies (1%) of fetal bovine serum (10%), penicillin, and streptomycin at 37°C, 5% CO_2. M2 TAMs were obtained by incubation in 1640 medium containing 20 ng mL^{-1} interleukin-4 (IL-4) for 12 h.

Cellular Uptake of $_{ER}Fe_3O_4$ NPs

The induced M2 TAMs were seeded in 6-well plates at a density of 1.6×10^5 cells per well (1.6 mL). Utilize a Halo counter cell counter for cell enumeration. The next day, replace the original cell culture medium with fresh medium containing 0, 25, 50, and 100 μg mL^{-1} of $_{ER}Fe_3O_4$ NPs (at the concentration of Fe_3O_4 NPs). Incubate for an additional 6 h, followed by 1–2 rinses with PBS, resuspension in fresh PBS, and subsequent centrifugation. Finally, 500 μL of aqua regia was added to dissolve the cells. After reducing the volume to 15 mL, the concentration of iron ions was detected by inductively coupled plasma-mass spectrometry (ICP-MS).

In vitro Toxicity Assessment Against TAMs, 4T1, and 3T3 Cells

Inoculate 1×10^4 cells in 100 μL per well in 96-well plates and incubate overnight. Subsequent to discarding the original medium and washing with PBS 1–2 times, introduce emodin (0–60 μg mL^{-1}), $_{R}Fe_3O_4$ NPs and $_{ER}Fe_3O_4$ NPs (0–200 μg mL^{-1}) for treatment. The 3-(4,5-dimethylthiazolyl-2)-2,5- diphenyltetrazolium bromide (MTT) was added to the culture for 3.5 h, and the microplate reader was used for detection.

In vitro Assessment of Lactate Production Inhibition

Raw 264.7 cells were initially seeded in a cell culture dish. The following day, the cell culture medium was replaced with fresh media containing PBS, emodin, $_{R}Fe_3O_4$, or $_{ER}Fe_3O_4$, and incubated for an additional 24 h. Subsequently, cells were collected after each treatment to measure pyruvic acid concentrations using a pyruvic acid detection kit.

TNF-α, IL-12, IFN-γ, TGF-β, IL-10 and Arg-1 Assessment

1×10^4 M2 TAMs per well (100 μL) are seeded overnight in 96-well plates. Add 0, 25, 50, and 100 μg mL^{-1} of $_{ER}Fe_3O_4$ NPs and $_{R}Fe_3O_4$ NPs containing 0, 7.5, 15, 30 μg mL^{-1} of emodin, and collect the supernatant 24 h later. Detected with enzyme linked immunosorbent assay (ELISA) (Biolegend).

CD16/32 and CD206 Expression

1×10^5 cells per well were seeded in 24-well plates. After being incubated with $_{R}Fe_3O_4$ NPs and $_{ER}Fe_3O_4$ NPs (equivalent to 100 μg mL^{-1} Fe_3O_4) for 24 h, the cells were subsequently washed twice with PBS and collected. Subsequently, the

cells redispersed in 500 μL PBS containing either PE/Cy7 anti-mouse CD16/32 antibody or PE anti-mouse CD206 antibody, stained for 15 min and performed by flow cytometry.

Detection of Cell Viability, Live/Dead Cell Staining and Apoptosis in the 4T1-M2 TAMs Co-Culture Transwell System

Seeding 1×10^5 M2 TAMs cells per well in the upper chamber in Transwell co-cultured 24-well plate. Simultaneously, seed 2.5×10^4 4T1 cells in the lower chamber, allowing them to culture overnight.[34] The following day, culture with emodin, $_{R}Fe_3O_4$ NPs and $_{ER}Fe_3O_4$ NPs (equivalent to 100 μg mL^{-1} Fe_3O_4 or 30 μg mL^{-1} emodin) for 24 h, and assess cell viability by MTT. To detect apoptosis, collect 4T1 cells using EDTA-free trypsin, wash with PBS, suspend the cells in binding buffer, and stain for 20–30 min using an apoptosis kit. Analyze the stained cells using flow cytometry. For fluorescence microscopy assay, cells were cultured with the Calcein AM/PI assay working solution at the appropriate volume. Incubate at 37°C in the dark for 30 min, and observe the resulting staining under a fluorescence microscope.

Establishment and Fluorescence Imaging of a 4T1 Tumor-Bearing Mouse Model

BALB/c mice (15–20 g, female, 6 weeks) were inoculated subcutaneously with 100 μL of PBS containing 2×10^6 4T1 cells. Animal experiments were conducted in accordance with the regulations of the China Animal Protection Committee, and the research plan was approved by the Experimental Animal Ethics Committee of Shandong First Medical University (No. W20205233228). When tumor volume reaches 150–200 mm^3, 100 μL of Cy5-loaded $_{R}Fe_3O_4$ NPs is injected through the mice's tail vein (equivalent to 0.5 mg Cy5 kg^{-1} mice).[39] After 24 h, conduct fluorescence imaging on the liver, spleen, lung, kidney, and tumor. In addition, the main organs and tumors are taken and thawed with 10 mL of concentrated nitric acid, diluted with ultrapure water and determined ionic concentration by ICP-MS.[40]

In vivo Assessment of Lactate Production Inhibition

Initially, 4T1 tumor cells were inoculated subcutaneously of BALB/c mice. Once the tumor volume reached approximately 400 mm^3, PBS, Emodin, $_{R}Fe_3O_4$ and $_{ER}Fe_3O_4$ NPs (100 μL) were intravenously injected into the mice. 24 h later, the tumors were collected and minced. Finally, the pyruvic acid levels were measured using a pyruvic acid assay kit.

Tumor Growth and Body Weight

Upon reaching a volume of tumor approximately 70 mm^3, the mice were randomly assigned to four groups: (a) PBS; (b) Emodin; (c) $_{R}Fe_3O_4$ NPs; and (d) $_{ER}Fe_3O_4$ NPs. The intravenous dosage administered was equivalent to 20 mg kg^{-1} for Fe_3O_4 NPs or 6 mg kg^{-1} for emodin in mice. Tumor volume was assessed by utilizing the formula ($width^2$ × length/2) based on measurements taken with a digital caliper. On the eighteenth day, mice were euthanized and dissected.

Analysis of Macrophages and T Cells of Mice

On the 8th day, tumor tissues were collected from each group, rinsed with cold PBS, and subsequently incubated in a solution containing Collagenase A and DNase I. Following digestion at 37°C for 45 min and termination on ice, filter the digested tissues through 70 μm nylon strainers to obtain single-cell suspensions. Before cell flow cytometry antibody staining, tumor cells were treated with PE/Cy7 anti-mouse CD16/32 and PE anti-mouse CD206. The immunofluorescence staining of CD16/32 and CD206 in tumor tissue were measured. Additionally, lymph nodes were stained with PE anti-mouse CD4 antibody and APC anti-mouse CD8 antibody. Treatments involved using FITC-anti-mouse CD80 antibody and PE anti-mouse CD86 antibody, followed by DAPI staining. Moreover, the tumors were sectioned and stained immunofluorescence, and then observed with a microscope.

Hematoxylin and Eosin Staining (H&E)

On the eighteenth day, the mice were euthanized, and their main organs (heart, liver, spleen, lung, and kidney) as well as tumors were excised. These samples were sectioned into 5 μm slices for H&E staining and examined using a digital microscope for pathological analysis.

Hemolysis Experiment

Mouse red blood cells were washed with PBS to remove serum, and then suspended in PBS (20 mL). $_{ER}Fe_3O_4$ NPs were added to the erythrocyte suspension at concentrations equivalent to 0, 20, 40, 60, 80, 100, 200 and 400 μg mL^{-1} Fe_3O_4 NPs. Positive controls were erythrocyte suspensions diluted with deionized water, while negative controls were those diluted with PBS.[41] Based on the aforementioned procedure, we assessed and computed the hemolysis rate after 1–3 h of incubation at 37°C.

Results

Synthesis and physicochemical characterization of $_{ER}Fe_3O_4$ NPs

The synthetic procedure for the $_{ER}Fe_3O_4$ NPs is visually presented in Figure 1. Hollow Fe_3O_4 NPs were prepared via a straightforward one-pot method that involved hydrothermal treatment of $FeCl_3$, polyacrylamide, citrate, and urea.[32] The SEM image demonstrated the rough surface of hollow Fe_3O_4 NPs (Figure 2a). Monodispersed, spherical and hollow structure of Fe_3O_4 NPs was revealed by TEM in Figure 2b, which is uniform with a diameter of 206.5 ± 15.3 nm. Next, DSPE-PEG2000-Gala-inserted red blood cell membrane (gRBCs) was employed to coat Fe_3O_4 NPs loaded with emodin, resulting in the synthesis of $_{ER}Fe_3O_4$ NPs. The TEM images depicting mRBCs (Figure S1a) and $_{ER}Fe_3O_4$ NPs (Figure S1b) show that continuous outer membrane shells are coated on the rough surface of $_{E}Fe_3O_4$ NPs, resulting in slightly increased size of $_{ER}Fe_3O_4$ NPs. The XRD analysis revealed a close match between the diffraction pattern of these NPs and the crystalline structure of Fe_3O_4 NPs (JCPDS 75–0033), as shown in Figure 2c. Additionally, energy-dispersive spectroscopy (EDS) element mapping analysis illustrated the uniform distribution of Fe and O in Figure 2d. Meanwhile, in the XPS spectrum (Figure 2e), the peaks corresponding to $Fe2p_{3/2}$ and $Fe2p_{1/2}$ are at binding energies of about 710.6 eV and 724.6 eV, respectively, which are consistent with previous Fe_3O_4 reported in literature.[32] As depicted in Figure 2f, the surface area and average pore diameter of hollow Fe_3O_4 NPs were 229.2 m^2/g and 16.4 nm, respectively, confirmed that hollow Fe_3O_4 is beneficial to encapsulate drugs for tumor therapy. Emodin was loaded into the hollow cavity of these Fe_3O_4 NPs through 24 h of incubation under absolute ethanol conditions. Thereafter, hollow Fe_3O_4 NPs could efficiently load emodin by HPLC analysis, and the loading ratio ([emodin]/[Fe_3O_4], w/w) was determined to be approximately 30% in Figure 2g. To further obtain $_{ER}Fe_3O_4$ NPs, $_{E}Fe_3O_4$ NPs were coated by gRBCs to improve the biocompatibility of these NPs and the biological targeting of M2-like TAMs. As illustrated in Figure 2h, sodium dodecyl sulfate- polyacrylamide gel electrophoresis (SDS-PAGE) was used to confirm the presence of membrane proteins. The results substantiated that the membrane proteins of gRBCs were preserved in large quantities for $_{R}Fe_3O_4$ NPs. Furthermore, DLS results showed that the average hydrodynamic diameter of Fe_3O_4 NPs increased from 205.7 ± 3.3 nm to 215.7 ± 6.5 nm, and further to 240.3 ± 5.0 nm post-encapsulation of gRBCs, demonstrating successful membrane encapsulation (Figure 2i). Concurrently, the zeta potentials of gRBCs (−8.5 mV), Fe_3O_4 NPs (−32.3 mV), $_{E}Fe_3O_4$ NPs (−41.1 mV), and $_{ER}Fe_3O_4$ NPs (−31.4 mV) were evaluated, reaffirming the successful encapsulation of gRBCs and loading of emodin for Fe_3O_4 NPs (Figure 2j). These results validate the successful formation of $_{ER}Fe_3O_4$ NPs and establish a solid basis for their efficient implementation.

The Ability to Reprogram M2 to M1 TAMs of $_{ER}Fe_3O_4$ NPs

Inhibition of lactate and exposure of iron have been demonstrated to reprogram M2-like TAMs to M1-like TAMs.[42,43] Under physiological conditions, the concentration of lactic acid in blood and healthy tissues is 1.5 to 3.0 mM. Nevertheless, lactate content in TME reaches 10 to 40 mM, which is affected by the active metabolism of glucose and glutamine in rapid-proliferation of tumor cells.[44] As illustrated in Figure 3a, the enzymatic conversion of pyruvate to lactate, facilitated by LDH activity, maintains the NADH/NAD^+ ratio and cytosolic levels of nicotinamide adenine dinucleotide (NAD^+) in order to sustain glycolytic flux.[45] Suppression of LDH activity could reduce ulteriorly lactate secretion. To explore the inhibitory impact of $_{ER}Fe_3O_4$ NPs on LDH, we exposed varying concentrations of $_{ER}Fe_3O_4$ NPs to buffer solutions containing pyruvate, NADH, and LDH. As illustrated in Figure 3b, the accumulation of converted pyruvate exhibited a progressive rise with escalating levels of $_{ER}Fe_3O_4$ NPs treatment, indicating the lactate inhibition effect of $_{ER}Fe_3O_4$ NPs. Simultaneously, different concentrations of $_{ER}Fe_3O_4$ NPs were introduced into the aforementioned reaction system. As depicted in Figure 3c, an increase in $_{ER}Fe_3O_4$ concentration corresponded to elevated NADH

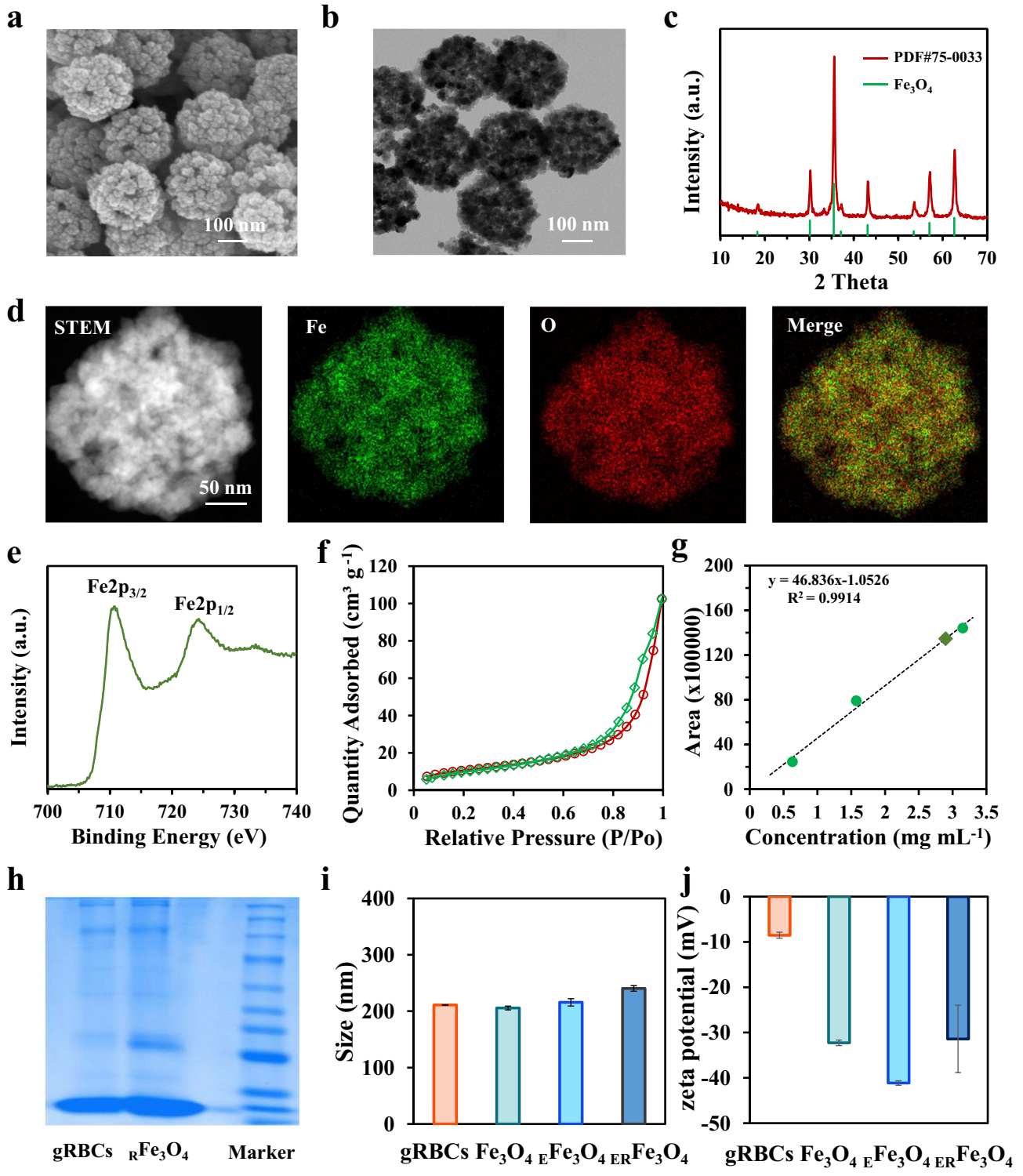

Figure 2 Physicochemical characterization of $_{ER}Fe_3O_4$ NPs. (**a**) SEM image and (**b**) TEM image of hollow Fe_3O_4 NPs. (**c**) XRD pattern, (**d**) STEM and the elemental mapping images of hollow Fe_3O_4 NPs. (**e**) XPS spectra of Fe2p region of hollow Fe_3O_4 NPs. (**f**) N_2 adsorption/desorption isotherm of hollow Fe_3O_4 NPs. (**g**) A calibration curve using HPLC spectroscopy was employed to assess the efficiency of emodin loading. (**h**) Protein analysis of gRBCs, $_{R}Fe_3O_4$ NPs and Marker by using SDS-PAGE. Samples were stained with Coomassie Brilliant. (**i**) Size and (**j**) Zeta potential of gRBCs, Fe_3O_4 NPs, $_{E}Fe_3O_4$ NPs and $_{ER}Fe_3O_4$ NPs.

accumulation. In summary, the findings demonstrated that $_{ER}Fe_3O_4$ NPs possess the capability to inhibit LDH, consequently curtailing lactic acid production. Subsequently, we evaluated the ability of $_{ER}Fe_3O_4$ NPs to promote a shift of M2-like TAMs to M1-like TAMs. To start with, we induced M0 macrophages (RAW 264.7) with IL-4 to repolarize them

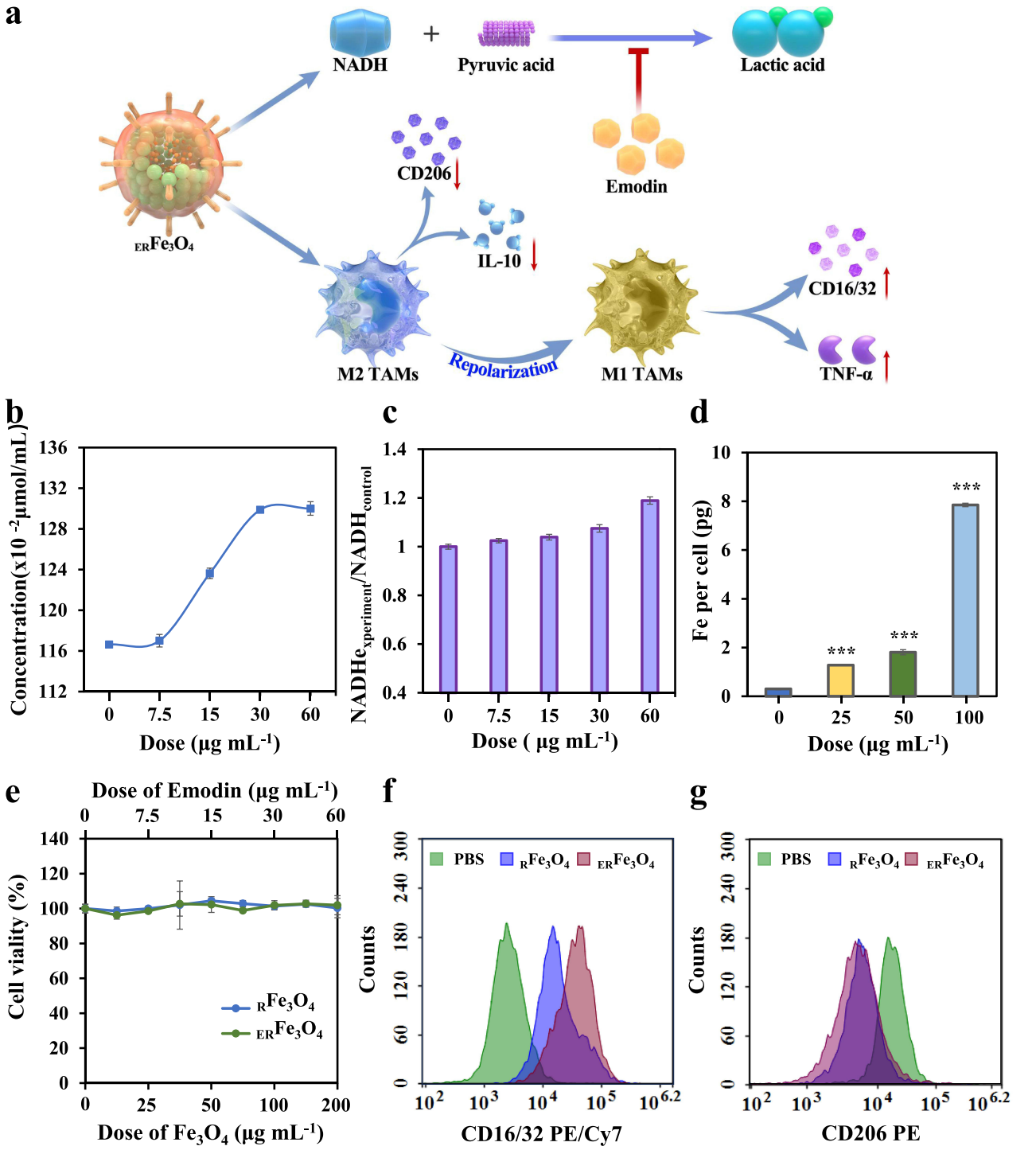

Figure 3 The characteristics of reprogramming of M2 to M1 TAMs for $_{ER}Fe_3O_4$ NPs. (**a**) Schematic illustration of reprogram M2 to M1 TAMs by $_{ER}Fe_3O_4$ NPs. (**b**) Quantitation of pyruvate under various dose of emodin (equivalent to 0, 25, 50, 100, 200 μg mL^{-1} $_{ER}Fe_3O_4$ NPs) was measured. (**c**) NADH depletion at different emodin concentrations (equivalent to 0, 25, 50, 100, 200 μg mL^{-1} $_{ER}Fe_3O_4$). (**d**) The cellular uptake of $_{ER}Fe_3O_4$ NPs at different doses was examined for 6 h, and the presence of Fe ions in the cells was detected using ICP-MS. The asterisk indicates statistical significance compared to the control group. *** $p < 0.001$. (**e**) The viability of M2 TAMs cells was assessed by MTT assay after 24 h of incubation with $_{R}Fe_3O_4$ and $_{ER}Fe_3O_4$ NPs. (**f** and **g**) Flow cytometry was used to analyze the expression of CD16/32 (PE/Cy7) and CD206 (PE) in of $F4/80^+$ macrophage treated with PBS, $_{R}Fe_3O_4$ NPs and $_{ER}Fe_3O_4$ NPs (equivalent to 100 μg mL^{-1} Fe_3O_4) for 24 h.

into M2-like TAMs. We then evaluated the cellular uptake of $_{ER}Fe_3O_4$ NPs in these cells using ICP-MS analysis. Figure 3d demonstrates the results of this analysis, the cellular iron level represented a dose-dependent elevation profile, manifesting the significant iron uptake in M2-like TAMs. Additionally, toxicities of $_{ER}Fe_3O_4$ NPs were evaluated by the MTT assay. No apparent toxicology induced by $_{R}Fe_3O_4$ and $_{ER}Fe_3O_4$ NPs was exhibited after 24 h incubation in

Figure 3e. Next, to assess cellular lactate inhibition capabilities, cells were collected for analysis following a 24 h treatment with PBS, emodin (30 μg mL^{-1}), $_{R}Fe_3O_4$, and $_{ER}Fe_3O_4$ NPs (100 μg mL^{-1}). Compared to the PBS and $_{R}Fe_3O_4$ NPs groups, treatment with emodin and $_{ER}Fe_3O_4$ NPs led to a pronounced increase in pyruvic acid concentration, indicating the intracellular inhibitory effect of emodin on lactate production (Figure S2). Subsequently, to further inquire the ability of $_{ER}Fe_3O_4$ NPs to reverse TIME, the expression of CD 16/32 and CD 206, specific markers for M1 and M2 phenotype, was evaluated by flow cytometric analysis. As shown in Figure 3f, $_{R}Fe_3O_4$ and $_{ER}Fe_3O_4$ NPs groups triggered increased the expression of CD16/32 compared with the PBS group, indicating an increase in M1 TAMs induction. Besides, $_{R}Fe_3O_4$ and $_{ER}Fe_3O_4$ NPs groups also significantly reduced the expression of CD206, implying a reduction induced by M2 TAMs in Figure 3g. These results substantiated that $_{ER}Fe_3O_4$ NPs exhibited the strongest M2-like TAMs repolarization activity and lay the foundation for anti-tumor immunotherapy.

In vitro Antitumor Effect of $_{ER}Fe_3O_4$ NPs

Proinflammatory M1-like TAMs have been reported to exert anti-tumor activity by secreting proinflammatory cytokines and reactive nitrogen or reactive oxygen species.[46] To further confirm the anti-tumor potential of M2-like TAMs that have been converted into M1-like TAMs, we utilized a 4T1-M2 TAMs transwell system for verification. As shown in Figure 4a, 4T1 cells and M2-like TAMs were co-cultured using a two-chamber transport system, wherein a 0.4 μm sized microporous membrane of chamber allowed the translocation of cytokines between the chambers (using a 0.4 μm size microwell membrane to study the effect of a substance secreted by cells on the growth of another cell). Following treatment with $_{ER}Fe_3O_4$ NPs, M2-like TAMs in the upper compartment were reprogrammed to M1-like TAMs. This resulted in an increase in the expression of certain pro-inflammatory factors, which could inhibit the growth of tumor cells. In the 4T1-M2 TAMs transwell system, cells in the upper and lower chambers were simultaneously incubated for 24 h with 100 μg mL^{-1} $_{R}Fe_3O_4$ NPs or $_{ER}Fe_3O_4$ NPs or emodin. The survival of 4T1 cells in the lower chamber was additionally assessed using an MTT assay. As shown in Figure 4b, $_{R}Fe_3O_4$ NPs could trigger 34.9% of 4T1 cells death on account of the induction of M1 polarization by Fe_3O_4 and the release of inflammatory factors, whereas $_{ER}Fe_3O_4$ NPs induced 54.7% cell death, which attribute to synergistic enhancement of M1 polarization effect by emodin. In contrast, the cell viabilities of 3T3 cells after $_{R}Fe_3O_4$ NPs or $_{ER}Fe_3O_4$ NPs incubation for 24 h among the concentrations of 0 to 200 μg mL^{-1} were all above 90%, implying the safety of $_{ER}Fe_3O_4$ NPs in vitro in Figure 4c. Besides, the cell live/dead double staining assay was used to further verify the killing effect of MTT on 4T1 cells, which had a similar trend with MTT in Figure 4d. In Figure 4e, the results of the fluorescein-annexin V and propidium iodide (PI) staining assays indicated that the impact of emodin, $_{R}Fe_3O_4$ NPs, or $_{ER}Fe_3O_4$ NPs on cell viability was primarily associated with apoptosis. Q1, Q2, Q3, and Q4 represent necrotic cells, late apoptotic cells, viable cells, and early apoptotic cells, respectively. The proportion of apoptotic cells treated with emodin, $_{R}Fe_3O_4$ NPs or $_{ER}Fe_3O_4$ NPs was 14.8%, 27.7% and 42.4%, respectively, indicating that the synergistic M2-like TAMs repolarization activity of emodin and Fe_3O_4 NPs could trigger significant 4T1 cell apoptosis. To further reveal the reasons for the cytotoxicity of $_{ER}Fe_3O_4$ NPs in 4T1-M2 TAMs transwell system, the direct toxicity of $_{ER}Fe_3O_4$ NPs on 4T1 cells was first evaluated by MTT assay. As presented in Figures 4f and S3, emodin (0–60 μg mL^{-1}), $_{R}Fe_3O_4$ NPs or $_{ER}Fe_3O_4$ NPs (0–200 μg mL^{-1}) presented low direct killing effect on 4T1 cells, which indicating the killing effect of $_{ER}Fe_3O_4$ NPs on 4T1 cells in the 4T1-M2 TAMs system was closely related to TAMs. It has been reported that M1-like TAMs may exert antitumor activity by secreting proinflammatory cytokines.[46] Reprogramming M2-like TAMs to an M1-like state inhibits the levels of IL-10, TGF-β, and Arg-1, while stimulating the secretion of pro-inflammatory factors, such as TNF-α, IL-12, and IFN-γ. This process was assessed using ELISA assays. Figure 4g and S4a-b illustrates significantly reduced levels of IL-10, TGF-β, and Arg-1 in the $_{ER}Fe_3O_4$ NPs group compared to other groups, potentially attributed to the synergistic release of emodin and Fe_3O_4 NPs. Conversely, analysis of pro-inflammatory factors TNF-α, IL-12, and IFN-γ using the same method is depicted in Figures 4h and S4c–d, highlighting the $_{ER}Fe_3O_4$ NPs group's pronounced promotional effect. These results substantiate that $_{ER}Fe_3O_4$ NPs can reprogram M2-like TAMs to induce the secretion of pro-inflammatory factors, thereby augmenting their cytotoxic impact on tumor cells.

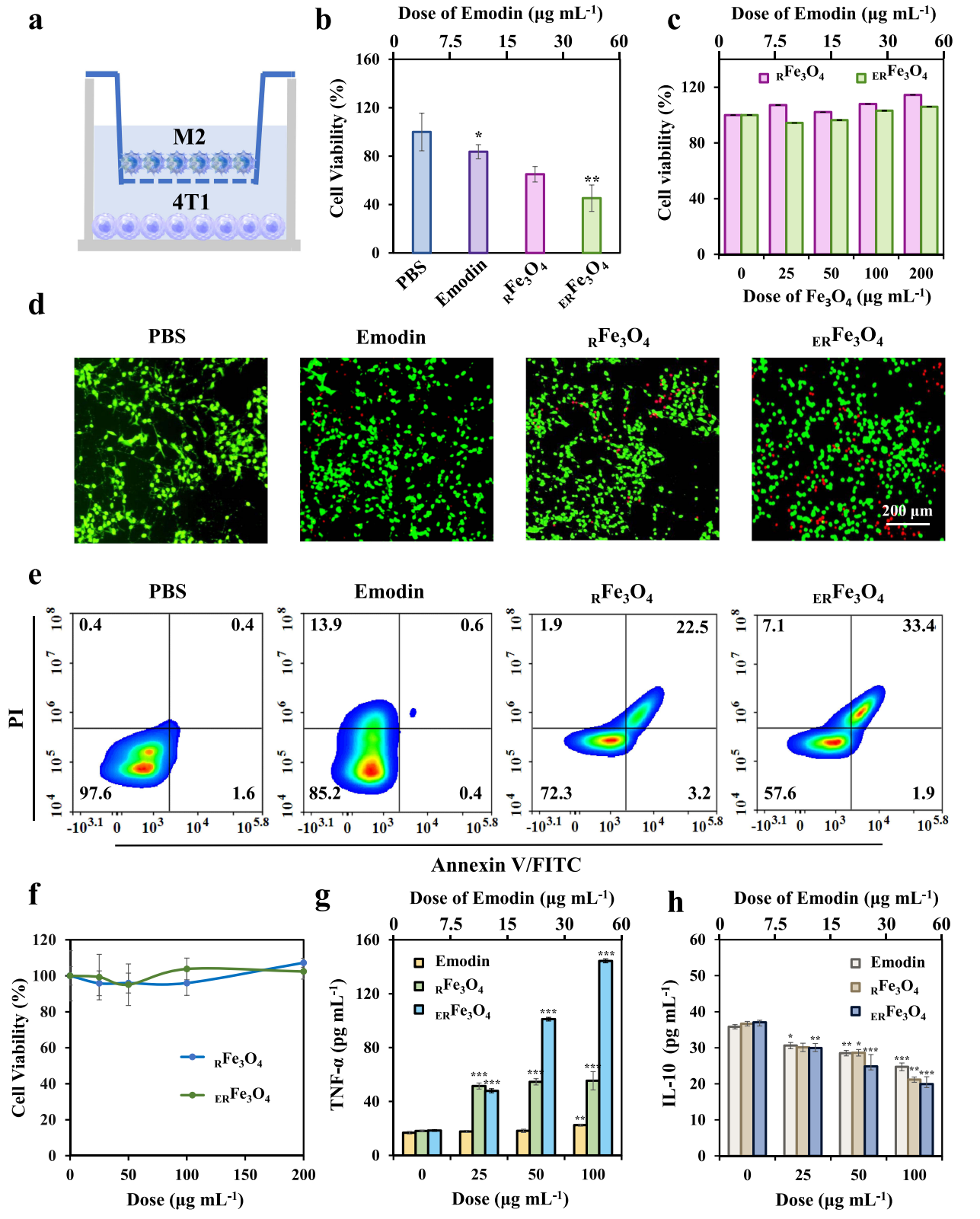

Figure 4 In vitro antitumor assessment of $_{ER}Fe_3O_4$ NPs. (**a**) Schematic diagram of 4T1-M2 TAMs co-culture transwell system. (**b**) The viability of 4T1 cell of 4T1-M2 TAMs co-culture transwell system. Statistical significance compared to the PBS group is indicated by the labeled asterisk. *p < 0.05, **p < 0.01. (**c**) The viability of 3T3 cells was assessed. (**d**) The staining of live and dead cells in 4T1 cell population of 4T1-M2 TAMs co-culture transwell system was performed. (**e**) Flow cytometric analysis was conducted on 4T1 cells that were treated with PBS, emodin, $_{R}Fe_3O_4$, or $_{ER}Fe_3O_4$ NPs of 4T1-M2 TAMs co-culture transwell system for a duration of 24 h. (**f**) Cell viability of 4T1 cells incubated with $_{R}Fe_3O_4$ and $_{ER}Fe_3O_4$ NPs for 24 h. (**g** and **h**) The TNF-α and IL-10 levels in M2 TAMs were measured after treatment with PBS, emodin, $_{R}Fe_3O_4$ NPs, and $_{ER}Fe_3O_4$ NPs for 24 h. The asterisk denotes statistical significance different concentrations compared to the control group, as determined by one-way ANOVA and Tukey's post-hoc test. * p < 0.05, ** p < 0.01, *** p < 0.001.

In vivo Therapeutic Effect of $_{ER}Fe_3O_4$ NPs

The cytotoxic effect of $_{ER}Fe_3O_4$ NPs on 4T1 cells in vitro prompted us to evaluate their potential for anti-tumor immunotherapy in vivo. First, nanomedicine could be further used for cancer treatment only if it is less toxic to humans. We evaluated their toxicity by hemolysis test, hematology analysis and H&E staining of heart, liver, spleen, lung, kidney tissues. As presented in Figure 5a, hemolysis rate of $_{ER}Fe_3O_4$ NPs at various concentrations was below 5%, which indicates the safety of $_{ER}Fe_3O_4$ NPs injection. The results of blood biochemical and hematological analysis of mice in each group were all within the reference range, and the increase or decrease of indexes was not large, showing good biocompatibility (Figures S5–S7). As shown in Figure S8, there was no significant toxicity by H&E staining of in the main organs after intravenous injection in different groups. These data further support the good biocompatibility of $_{ER}Fe_3O_4$ NPs in vivo. At the same time, fluorescence images and ICP-MS were used to observe the biodistribution of $_{ER}Fe_3O_4$ NPs after 24 h intravenous injection. As exhibited in Figure 5b, Cy5-loaded $_{R}Fe_3O_4$ NPs have a significant accumulation in tumor tissues. According to Figure 5c, the predominant distribution of $_{ER}Fe_3O_4$ NPs after 24 h injection was observed in the spleen and lungs, and showed obvious accumulation behavior in tumors. Significant fluorescence intensity was notably observed in spleen, lung, and kidney tissues, likely due to the nanoparticles' slightly larger size and the crucial metabolic roles played by these organs. Next, we evaluated the in vivo efficacy of lactate production inhibition. Tumor-bearing mice were intravenously injected separately with PBS, Emodin, $_{R}Fe_3O_4$, and $_{ER}Fe_3O_4$ NPs. Tumor tissues were collected and homogenized 24 h post-injection for pyruvic acid monitoring. As anticipated, the free emodin exhibited lower efficacy due to its limited tumor-targeting capability compared to $_{ER}Fe_3O_4$ NPs. In contrast, $_{ER}Fe_3O_4$ NPs, benefiting from their tumor-targeting and prolonged retention properties, resulted in higher pyruvic acid concentrations in treated mice compared to other groups (Figure S9). This outcome underscores $_{ER}Fe_3O_4$ NPs effective inhibition of lactate production. Overall, these findings highlight $_{ER}Fe_3O_4$ NPs successful accumulation at tumor sites, contributing to the mitigation of the acidic tumor microenvironment. In the schematic diagram of Figure 5d, 4T1 tumor-bearing mice were intravenously injected with PBS, emodin, $_{R}Fe_3O_4$ NPs, or $_{ER}Fe_3O_4$ NPs (equivalent to 20 mg Fe_3O_4 or 6 mg emodin per kg^{-1} mouse) on days 1, 3, and 5. As shown in Figure 5e, intravenous injection of $_{ER}Fe_3O_4$ NPs had no significant effect on the body weight of mice during treatment. After treatment, the anti-tumor effect was most significant in the $_{ER}Fe_3O_4$ NPs group (Figures 5f, S10 and S11).

To further elucidate the therapeutic efficacy of $_{ER}Fe_3O_4$ NPs, histological analysis of tumors was performed using H&E staining. The pathological alterations in tumor sections after completion of the treatment were evaluated in Figure 5g. $_{ER}Fe_3O_4$ NPs showed an excellent therapeutic effect with the most severe tumor cell apoptosis and necrosis. To better clarify the function of immunotherapy in combatting tumors, the fluorescence intensity of $CD4^+$ and $CD8^+$ T cells in tumor exhibited a significantly higher level compared to other treatment groups under $_{ER}Fe_3O_4$ NPs treatment as depicted in Figure S12. Moreover, Figure 5h demonstrates a notable enhancement in DCs maturation within $_{ER}Fe_3O_4$ NPs treated tumors, as evidenced by immunofluorescence staining. In addition, flow cytometry was utilized to determine the proportion of $CD4^+$ or $CD8^+$ T lymphocytes in tumor draining lymph nodes. As shown in Figure S13, a large number of $CD4^+$ and $CD8^+$ T cells could be explored in tumor draining lymph nodes on the 8th day. The different groups treated with PBS, emodin, $_{R}Fe_3O_4$ NPs, or $_{ER}Fe_3O_4$ NPs showed $CD8^+$ T lymphocytes infiltration rates of 10.3%, 11.2%, 18.0%, and 23.9%, and 24.5%, 37.0%, 44.1%, and 52.3% of $CD4^+$ T lymphocytes, respectively. Furthermore, flow cytometry analysis be conducted to evaluate the expression levels of CD16/32 and CD206 in $F4/80^+$ macrophages, which serves as a reliable marker for intertumoral macrophages. The outcomes demonstrated that $_{ER}Fe_3O_4$ NPs induced elevated CD16/32 expression and reduced CD206 expression compared to PBS, emodin, and $_{R}Fe_3O_4$ NPs. As depicted in Figure 5i and 5j, the expression of CD16/32 was 22.4%, 27.8%, 30.0% and 54.8% after different treatments, respectively. The expressions of CD206 were 16.9%, 13.2%, 5.9% and 3.5%, respectively, indicating that $_{ER}Fe_3O_4$ NPs have excellent TME reprogramming ability in vivo. Subsequently, immunofluorescence was employed to visually assess phenotype transformation. CD206 served as a biomarker for M2 macrophages, whereas CD16/32 was utilized as a biomarker for M1 macrophages. Compared with other groups, $_{ER}Fe_3O_4$ NPs exhibited reduced CD206 fluorescence signal and elevated CD16/32 fluorescence signal (Figure S14). These results confirm that $_{ER}Fe_3O_4$ NPs treatment can activate an anti-tumor immune response based on macrophages and T cells. Therefore, activating the immune stimulating microenvironment

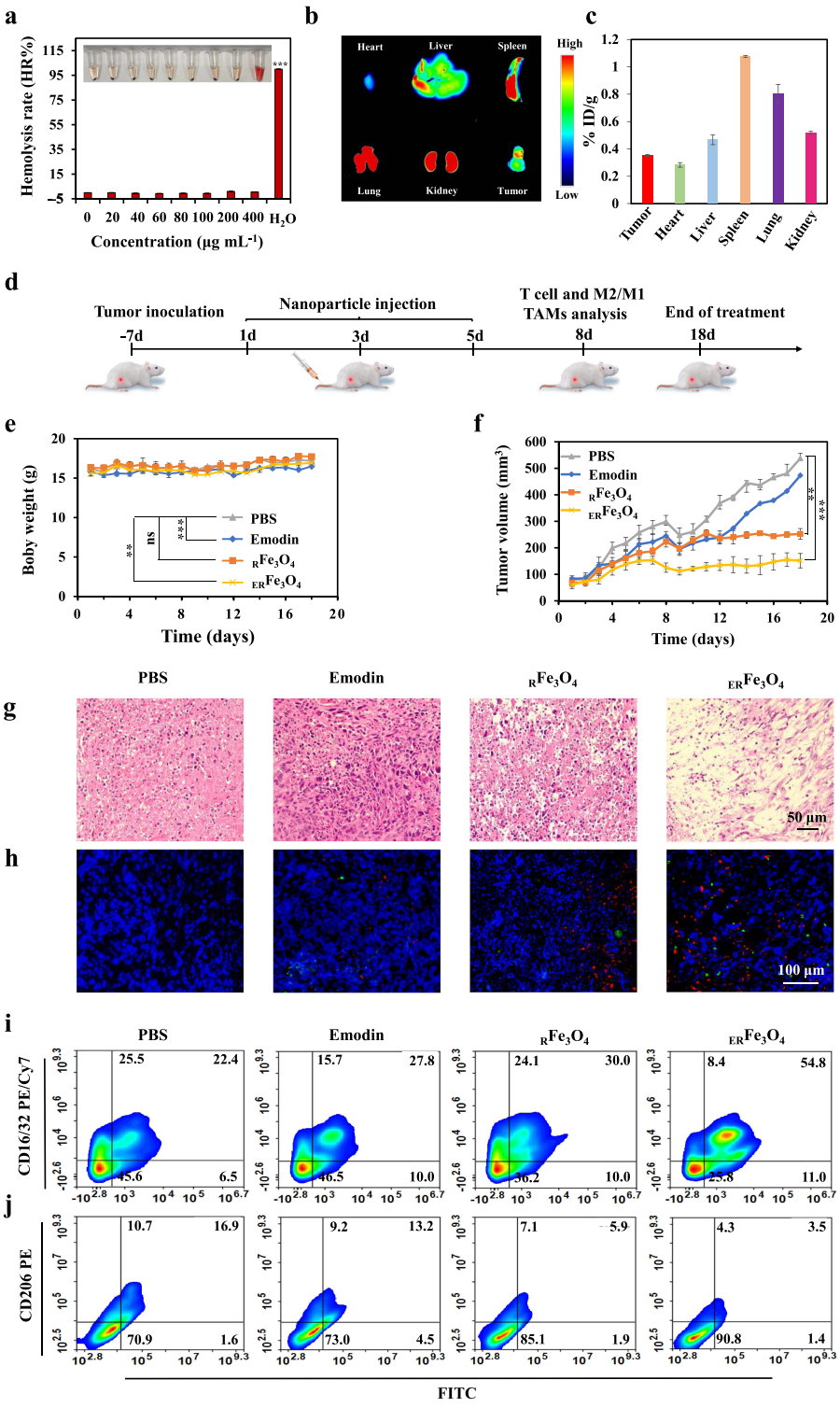

Figure 5 In vivo evaluation of the anticancer and immunotherapeutic effects of $_{ER}Fe_3O_4$ NPs. (**a**) Digital photograph of hemolysis test and quantification of hemolysis rate (HR%) of $_{ER}Fe_3O_4$ NPs. (**b**) Fluorescence imaging of major organs and tumor 24 h post-injection of $_{ER}Fe_3O_4$ NPs. (**c**) The concentrations of Fe ions in mouse tissues and tumor were measured via ICP-MS analysis after 24 h administration of $_{ER}Fe_3O_4$ NPs. The results were presented as the percentage of the injected dose per gram of tissue (% ID/g). (**d**) Schematic diagram of timeline depicting the treatment process of PBS, emodin, $_{R}Fe_3O_4$ NPs, or $_{ER}Fe_3O_4$ NPs. (**e**) The body weight change of mouse during the treatment period. (**f**) Tumor growth curves were plotted for a 4T1 tumor-bearing mouse model treated with various nanoparticles (n = 6). (**g**) After 18 days of treatment, tumor tissue was stained using H&E. (**h**) Immunofluorescence stained of CD80 and CD86 in tumor tissue on the 8th day (Red: CD80. Green: CD86). (**i** and **j**) Flow cytometry was used to analyze the levels of CD16/32 and CD206 in F4/80$^+$ macrophages within tumor tissues. In (**a**), (**e**), and (**f**), asterisks indicate statistical significance compared to the PBS group, as determined by one-way ANOVA with Tukey's post-hoc analysis. ** $p < 0.01$, *** $p < 0.001$.

can secrete more inflammatory factors, this facilitates the infiltration of $CD8^+$ and $CD4^+$ T cells into the tumor site, thus enhancing the efficacy of immunotherapy against tumor.

Discussion

Tumor-infiltrating immune cells usually experience metabolic stress due to dysregulated metabolic activity of tumor cells, which leads to impaired anti-tumor immune responses. The abnormal bioenergetic activity of tumor cells utilize large amounts of glucose to produce lactate via glycolysis.[47] Clinical data from 311 patients showed that serum LDH levels higher than 1000 international units (IU)/l predicted advanced or metastatic disease.[48] Glucose consumption and lactate accumulation, interrupt the ability of macrophages to proinflammatory polarization and therefore promote the development of M2-like macrophages. Interestingly, tumor-bearing mice deficient in lactate dehydrogenase A (LDHA), had reduced numbers of spleen myeloid - derived suppressor cells (MDSCs) and increased cytotoxic function of tumor-infiltrating natural killer (NK) cells, indicating that lactate production facilitated tumor growth and impaired innate immune responses.[49] LDHA-mediated lactate production inhibits IFN-γ expression in tumor-infiltrating T cells and NK cells, thereby promoting tumor deterioration and immune escape in mouse models.[50] Thus, drugs that target tumor metabolism may synergistically enhance immunotherapy through metabolic reprogramming of the TME.

The TME harbors a pivotal constituent in the form of TAMs, typically linked with unfavorable prognosis and resistance to drugs.[51,52] Given TAMs' roles in promoting tumors, diverse strategies have been devised to counteract their impact. Researchers, in their pursuit of TAMs, have concentrated on transforming tumor-promoting M2-type macrophages into tumoricidal M1 macrophages, deeming it a potentially more advantageous approach.[53] Zanganeh et al illustrated that exposure to iron induces M1 polarization, overpowering concomitant anti-inflammatory M2 responses.[53,54] Iron-based nanoparticles have emerged as pivotal translational entities in confronting TAMs that foster immune responses and sensitize tumors to immunotherapies safely and effectively, such as MNPs@MDSCs,[55] Fe@PDA-PEG,[56] and PLGA-ION-R837@M.[57] Thus, we employed a nanoplatform backbone comprising hollow iron oxide to cooperatively induce the polarization of the M1 TAMs phenotype. Another distinctive trait of cancer cells involves the incessant generation of lactic acid through aerobic glycolysis, promoting TAMs polarization toward the M2 phenotype, intensifying immunosuppression within the TME and resulting in hypoxia.[58] Consequently, scientists posit that curtailing lactic acid production will effectively restore the immunosuppressive TME.

Emodin, an anthraquinone derivative extracted from rhubarb root, has a variety of biological functions, including anti-inflammatory, anti-oxidation, anti-cancer and neuroprotection.[59] We utilized magnetic hollow Fe_3O_4 NPs as a carrier to deliver emodin to the tumor microenvironment to overcome the problem of hydrophobicity of emodin. The introduction of emodin successfully suppressed the production of LDH, resulting in decreased lactic acid levels and facilitating the transformation of M2 TAMs into M1 TAMs.[22] This reprogramming from immunosuppression to immune stimulation enhances the effectiveness of tumor immunotherapy and holds promise for clinical applications.

Conclusion

Taken together, we synthesized an iron-based nanoplatform ($_{ER}Fe_3O_4$ NPs) in which natural product were loaded with hollow Fe_3O_4 NPs of gRBCs cloaks. This approach could not only assist the delivery of emodin with high efficacy to inhibit and neutralize tumor acidification but also synergistically switch M2 TAMs into M1 TAMs for cancer metabolic immunotherapy improvement.

Data Sharing Statement

Data will be made available on request from the corresponding author.

Acknowledgments

This study was supported by the National Natural Science Foundation of China (22207066), Shandong Provincial Natural Science Foundation (ZR2023QB273), Traditional Chinese Medicine Science and Technology Project of Shandong Province (Q-2022142, Q-2023096) and Shandong First Medical University Youth Science Foundation

Cultivation Funding Program (202201-026). Project for Scientific Research Innovation Team of Young Scholars in Colleges and Universities of Shandong Province (2022KJ196).

Author Contributions

All authors made a significant contribution to the work reported, whether that is in the conception, study design, execution, acquisition of data, analysis and interpretation, or in all these areas; took part in drafting, revising or critically reviewing the article; gave final approval of the version to be published; have agreed on the journal to which the article has been submitted; and agree to be accountable for all aspects of the work.

Disclosure

The authors declare that they have no known competing financial interests or personal relationships that could have appeared to influence the work reported in this paper.

References

1. Wang Y, Wang B, Li K, Wang M, Xiao H. Engineered metal and their complexes for nanomedicine-elicited cancer immunotherapy. *Mater Today Adv*. 2022. doi:10.1016/j.mtadv.2022.100276
2. Tian Y, Liu Z, Wang J, et al. Nanomedicine for Combination Urologic Cancer Immunotherapy. *Pharmaceutics*. 2023;15(2):546. doi:10.3390/pharmaceutics15020546
3. Zhang ZZ, Pan Z, Li QS, et al. Rational design of ICD-inducing nanoparticles for cancer immunotherapy. *Sci Adv*. 2024;106:1.
4. Sun B, Hyun H, Li L-T, Wang AZ. Harnessing nanomedicine to overcome the immunosuppressive tumor microenvironment. *Acta Pharmacol Sin*. 2020;41(7):970–985. doi:10.1038/s41401-020-0424-4
5. Chen W. On nano-solutions to overcome cancer hypoxia and resistance. *Nano TransMed*. 2023;2(1):e9130020. doi:10.26599/ntm.2023.9130020
6. Wang H, Ouyang W, Liu H. Tumor microenvironment responsive nanozymes for multimodal imaging of tumors. *Nano TransMed*. 2024;3:100032. doi:10.1016/j.ntm.2024.100032
7. Cassetta L, Pollard JW. Targeting macrophages: therapeutic approaches in cancer. *Nat Rev: Drug Discov*. 2018;17(12):887–904. doi:10.1038/nrd.2018.169
8. Wei X, Song M, Jiang G, et al. Progress in advanced nanotherapeutics for enhanced photodynamic immunotherapy of tumor. *Theranostics*. 2022;12(12):5272–5298.
9. Chen B, Guo K, Zhao X, et al. Tumor microenvironment-responsive delivery nanosystems reverse immunosuppression for enhanced CO gas/immunotherapy. *Exploration*. 2023;3(6). doi:10.1002/exp.20220140
10. Xiang X, Wang J, Lu D, Xu X. Targeting tumor-associated macrophages to synergize tumor immunotherapy. *Signal Transduct Target Ther*. 2021;6(1):75. doi:10.1038/s41392-021-00484-9.
11. Togashi Y, Shitara K, Nishikawa H. Regulatory T cells in cancer immunosuppression - implications for anticancer therapy. *Nat Rev Clin Oncol*. 2019;16(6):356–371. doi:10.1038/s41571-019-0175-7
12. Wei X, Wang J, Liang M, Song M. Development of functional nanomedicines for tumor associated macrophages-focused cancer immunotherapy. *Theranostics*. 2022;12(18):7821–7852. doi:10.7150/thno.78572
13. Chen F, Pu F. Implantable immune stents: a new opportunity for cancer treatment. *Biomater Transl*. 2023;4(1):3–4. doi:10.12336/biomatertransl.2023.01.002
14. Zhou X, Ma E, Zhang Y, et al. NIR-actuated targeted janus nanomotors remodel immunosuppressive tumor microenvironment for augmented cancer immunotherapy. *Adv Healthcare Mater*. 2023. doi:10.1002/adhm.202302272
15. Ummarino A, Allavena A. Current strategies to target tumor-associated-macrophages to improve anti-tumor immune responses. *Cells*. 2019;9(1). doi:10.3390/cells9010046
16. Angelin A, Gil-de-Gómez L, Dahiya S, et al. Foxp3 reprograms t cell metabolism to function in low-glucose, high-lactate environments. *Cell Metab*. 2017;25(6):1282–1293.e1287. doi:10.1016/j.cmet.2016.12.018
17. Lee KH, Lee MS, Cha EY, et al. Inhibitory effect of emodin on fatty acid synthase, colon cancer proliferation and apoptosis. *Mol Med Rep*. 2017;15(4):2163–2173. doi:10.3892/mmr.2017.6254
18. Iwanowycz S, Wang J, Hodge J, et al. Emodin inhibits breast cancer growth by blocking the tumor-promoting feedforward loop between cancer cells and macrophages. *Mol Cancer Ther*. 2016;15(8):1931–1942. doi:10.1158/1535-7163.MCT-15-0987
19. Rani R, Kumar V. Recent update on human lactate dehydrogenase enzyme 5 (hLDH5) inhibitors: a promising approach for cancer chemotherapy. *J Med Chem*. 2016;59(2):487–496. doi:10.1021/acs.jmedchem.5b00168
20. Granchi C, Fortunato S, Meini S, et al. Characterization of the saffron derivative crocetin as an inhibitor of human lactate dehydrogenase 5 in the antiglycolytic approach against cancer. *J Agr Food Chem*. 2017;65(28):5639–5649. doi:10.1021/acs.jafc.7b01668
21. Tao Y, Zhang Y, Cheng Y, Wang Y. Rapid screening and identification of α-glucosidase inhibitors from mulberry leaves using enzyme-immobilized magnetic beads coupled with HPLC/MS and NMR. *Biomed Chromatogr*. 2012;27(2):148–155. doi:10.1002/bmc.2761
22. Yin J, Zhao X, Chen X, Shen G. Emodin suppresses hepatocellular carcinoma growth by regulating macrophage polarization via microRNA-26a/transforming growth factor beta 1/protein kinase B. *Bioengineered*. 2022;13(4):9549–9564. doi:10.1080/21655979.2022.2061295
23. Li CX, Zhang Y, Dong X, et al. Artificially reprogrammed macrophages as tumor-tropic immunosuppression-resistant biologics to realize therapeutics production and immune activation. *Adv Mater*. 2019;31(15). doi:10.1002/adma.201807211
24. Zanganeh S, Hutter G, Spitler R, et al. Iron oxide nanoparticles inhibit tumour growth by inducing pro-inflammatory macrophage polarization in tumour tissues. *Nat Nanotechnol*. 2016;11(11):986–994. doi:10.1038/nnano.2016.168

25. Zhang Y, Liu S, Li D, et al. Adoptive transfer of Fe3O4-SWCNT engineered M1-like macrophages for magnetic resonance imaging and enhanced cancer immunotherapy. *Colloids Surf, B*. 2023;229:113452. doi:10.1016/j.colsurfb.2023.113452
26. Cieslewicz M, Tang J, Yu JL, et al. Targeted delivery of proapoptotic peptides to tumor-associated macrophages improves survival. *Proc Natl Acad Sci*. 2013;110(40):15919–15924. doi:10.1073/pnas.1312197110
27. Gao W, Hu CMJ, Fang RH, et al. Surface functionalization of gold nanoparticles with red blood cell membranes. *Adv Mater*. 2013;25 (26):3549–3553. doi:10.1002/adma.201300638
28. Huang Z, Zhang Z, Jiang Y, et al. Targeted delivery of oligonucleotides into tumor-associated macrophages for cancer immunotherapy. *J Control Release*. 2012;158(2):286–292. doi:10.1016/j.jconrel.2011.11.013
29. Ward SE, O'Sullivan JM, Drakeford C, et al. A novel role for the macrophage galactose-type lectin receptor in mediating von Willebrand factor clearance. *Blood*. 2018;131(8):911–916. doi:10.1182/blood-2017-06-787853
30. Zhang N, Zheng X, Couvee G, et al. Galactose supramolecular docking orchestrates macrophage phenotype. *Cell Mol Immunol*. 2020;17 (10):1111–1113. doi:10.1038/s41423-019-0358-2
31. Tang Y, Tang Z, Li P, et al. Precise Delivery of nanomedicines to M2 Macrophages by Combining "Eat Me/Don't Eat Me" Signals and its anticancer application. *ACS Nano*. 2021;15(11):18100–18112. doi:10.1021/acsnano.1c06707
32. Cheng W, Tang K, Qi Y, Sheng J, Liu Z. One-step synthesis of superparamagnetic monodisperse porous Fe3O4 hollow and core-shell spheres. *J Mater Chem*. 2010;20. doi:10.1039/b919164j
33. Cheng K, Sun Z, Zhou Y, et al. Preparation and biological characterization of hollow magnetic Fe3O4@C nanoparticles as drug carriers with high drug loading capability, pH-control drug release and MRI properties. *Biomater Sci*. 2013;1(9):965. doi:10.1039/c3bm60087d
34. Wu X, Cheng Y, Zheng R, et al. Immunomodulation of tumor microenvironment by arginine-loaded iron oxide nanoparticles for gaseous immunotherapy. *ACS Appl Mater Interfaces*. 2021;13(17):19825–19835. doi:10.1021/acsami.1c04638
35. Liu WL, Liu T, Zou MZ, et al. Aggressive man-made red blood cells for hypoxia-resistant photodynamic therapy. *Adv Mater*. 2018;30(35): e1802006. doi:10.1002/adma.201802006
36. Ding L, Wu Y, Wu M, et al. Engineered red blood cell biomimetic nanovesicle with oxygen self-supply for near-infrared-II fluorescence-guided synergetic chemo-photodynamic therapy against hypoxic tumors. *ACS Appl Mater Interfaces*. 2021;13(44):52435–52449. doi:10.1021/acsami.1c19096
37. Zhang L, Wang Z, Zhang Y, et al. Erythrocyte membrane cloaked metal–organic framework nanoparticle as biomimetic nanoreactor for starvation-activated colon cancer therapy. *ACS Nano*. 2018;12(10):10201–10211. doi:10.1021/acsnano.8b05200
38. Tian N, Sun W, Guo X, et al. Mitochondria targeted and NADH triggered photodynamic activity of chloromethyl modified Ru(ii) complexes under hypoxic conditions. *Chem Commun*. 2019;55(18):2676–2679. doi:10.1039/c8cc09186b
39. He Q, Zheng R, Ma J, et al. Responsive manganese-based nanoplatform amplifying cGAS-STING activation for immunotherapy. *Biomater Res*. 2023;27(1). doi:10.1186/s40824-023-00374-x
40. Chang Y, Feng Y, Cheng Y, et al. Anisotropic plasmonic metal heterostructures as theranostic nanosystems for near infrared light-activated fluorescence amplification and phototherapy. *Adv Sci*. 2019;6(11). doi:10.1002/advs.201900158
41. Sang Y, Cao F, Li W, et al. Bioinspired construction of a nanozyme-based H2O2 homeostasis disruptor for intensive chemodynamic therapy. *J Am Chem Soc*. 2020;142(11):5177–5183. doi:10.1021/jacs.9b12873
42. Zhao S, Li H, Liu R, et al. Nitrogen-centered lactate oxidase nanozyme for tumor lactate modulation and microenvironment remodeling. *J Am Chem Soc*. 2023;145(18):10322–10332. doi:10.1021/jacs.3c02005
43. Wei Z, Zhang X, Zhang Z, et al. Engineered iron-based nanoplatform amplifies repolarization of M2-like tumor-associated macrophages for enhanced cancer immunotherapy. *Chem Eng J*. 2022;433:133847. doi:10.1016/j.cej.2021.133847
44. Zhang Z, Zhong H, Zhou Y, et al. Lactate-driving Pt nanoflower with positive chemotaxis for deep intratumoral penetration. *Nano Today*. 2022. doi:10.1016/j.nantod.2022.101542
45. Hermans D, Gautam S, García-Cañaveras JC, et al. Lactate dehydrogenase inhibition synergizes with IL-21 to promote CD8+ T cell stemness and antitumor immunity. *Proc Natl Acad Sci*. 2020;117(11):6047–6055. doi:10.1073/pnas.1920413117
46. Zhang S-Y, Song X-Y, Li Y, et al. Tumor-associated macrophages: a promising target for a cancer immunotherapeutic strategy. *Pharmacol Res*. 2020:161. doi:10.1016/j.phrs.2020.105111.
47. Tseng SJ, Kempson IM, Huang K-Y, et al. Targeting tumor microenvironment by bioreduction-activated nanoparticles for light-triggered virotherapy. *ACS Nano*. 2018;12(10):9894–9902. doi:10.1021/acsnano.8b02813
48. Husain Z, Huang Y, Seth P, Sukhatme VP. Tumor-derived lactate modifies antitumor immune response: effect on myeloid-derived suppressor cells and NK cells. *J Immunol*. 2013;191(3):1486–1495. doi:10.4049/jimmunol.1202702
49. Zhang Z, Li B, Xie L, et al. Metal-phenolic network-enabled lactic acid consumption reverses immunosuppressive tumor microenvironment for sonodynamic therapy. *ACS Nano*. 2021;15(10):16934–16945. doi:10.1021/acsnano.1c08026
50. Zeng W, Li F, Jin S, et al. Functional polarization of tumor-associated macrophages dictated by metabolic reprogramming. *J Exp Clin Cancer Res*. 2023;42(1). doi:10.1186/s13046-023-02832-9
51. Mohammadi AT, Mohagheghi SZ, Farid AS, et al. *Cancer Textbook 4:(Cancer Treatment and Ovarian Cancer)*. Nobel Science; 2023. doi:10.3390/cancers
52. Komohara Y, Jinushi M, Takeya M. Clinical significance of macrophage heterogeneity in human malignant tumors. *Cancer Sci*. 2013;105(1):1–8. doi:10.1111/cas.12314
53. Mantovani A, Ponzetta A, Inforzato A, Jaillon S. Innate immunity, inflammation and tumour progression: double-edged swords. *J Internal Med*. 2019;285(5):524–532. doi:10.1111/joim.12886
54. Sindrilaru A, Peters T, Wieschalka S, et al. An unrestrained proinflammatory M1 macrophage population induced by iron impairs wound healing in humans and mice. *J Clin Investig*. 2011;121(3):985–997. doi:10.1172/jci44490
55. Yu G-T, Rao L, Wu H, et al. Myeloid-derived suppressor cell membrane-coated magnetic nanoparticles for cancer theranostics by inducing macrophage polarization and synergizing immunogenic cell death. *Adv Funct Mater*. 2018;28(37):1801389. doi:10.1002/adfm.201801389
56. Rong L, Zhang Y, Li W-S, et al. Iron chelated melanin-like nanoparticles for tumor-associated macrophage repolarization and cancer therapy. *Biomaterials*. 2019;225:119515. doi:10.1016/j.biomaterials.2019.119515

57. Liu L, Wang Y, Guo X, Zhao J, Zhou S. A biomimetic polymer magnetic nanocarrier polarizing tumor-associated macrophages for potentiating immunotherapy. *Small*. 2020;16(38):2003543. doi:10.1002/smll.202003543
58. Wei X, Song M, Jin G, et al. Multidimensional profiling of functionalized photothermal nanoplatforms for synergistic cancer immunotherapy: design, strategy, and challenge. *Coord Chem Rev*. 2024:499. doi:10.1016/j.ccr.2023.215488.
59. Wang W-B, Li J-T, Hui Y, et al. Combination of pseudoephedrine and emodin ameliorates LPS-induced acute lung injury by regulating macrophage M1/M2 polarization through the VIP/cAMP/PKA pathway. *Chinese Med*. 2022;17(1). doi:10.1186/s13020-021-00562-8